

A EUROPEAN JOURNAL

CHEMPHYSCHEM

OF CHEMICAL PHYSICS AND PHYSICAL CHEMISTRY

Accepted Article

Title: Synthesis, Optical and Theoretical Study of Alternated Ethylenedioxythiophene-pyridine Oligomers: Evolution from Planar Conjugated over Helicoidal towards Chiral Configuration

Authors: Floris Chevalier; Marina Charlot; Florence Mongin; Benoît Champagne; Edith Franz; Koen Clays; Mireille Blanchard-Desce

This manuscript has been accepted after peer review and the authors have elected to post their Accepted Article online prior to editing, proofing, and formal publication of the final Version of Record (VoR). This work is currently citable by using the Digital Object Identifier (DOI) given below. The VoR will be published online in Early View as soon as possible and may be different to this Accepted Article as a result of editing. Readers should obtain the VoR from the journal website shown below when it is published to ensure accuracy of information. The authors are responsible for the content of this Accepted Article.

To be cited as: ChemPhysChem 10.1002/cphc.201601057

Link to VoR: <http://dx.doi.org/10.1002/cphc.201601057>

A Journal of



www.chemphyschem.org

WILEY-VCH

Synthesis, Optical and Theoretical Study of Alternated Ethylenedioxythiophene-pyridine Oligomers: Evolution from Planar Conjugated over Helicoidal towards Chiral Configuration

Floris Chevallier,^{*,[a,b]} Marina Charlot,^[a] Florence Mongin,^[a,b] Benoît Champagne,^{*,[c]}
Edith Franz,^[d] Koen Clays,^{*,[d]} and Mireille Blanchard-Desce^{*,[a,e]}

[a] Chimie et Photonique Moléculaires, UMR 6510 CNRS - Université de Rennes 1, 35042 Rennes, France.

[b] Institut des Sciences Chimiques de Rennes, UMR 6226 CNRS - Université de Rennes 1, 35042 Rennes, France.

[c] Laboratoire de Chimie Théorique, Université de Namur, B-5000 Namur, Belgium.

[d] Department of Chemistry, University of Leuven, B-3001 Leuven, Belgium

[e] Univ. Bordeaux, Institut des Sciences Moléculaires (UMR 5255 CNRS), 33405 Talence, France.

e-mail addresses: floris.chevallier@univ-rennes1.fr, benoit.champagne@unamur.be,

koen.clays@fys.kuleuven.be, mireille.blanchard-desce@u-bordeaux.fr

Abstract

A series of alternated 3,4-ethylenedioxythiophene-alkynylpyridine oligomers (DA)_n with increased solubility has been synthesized and their photophysical properties and nonlinear optical properties have been investigated. Their quadratic polarizabilities β have been determined by performing HRS experiments to get information on their conformation in solution. These chromophores based on the alternation of electron-rich (D) and electron-poor (A) moieties exhibit optical properties that find their genesis in the combination of dipolar and helicoidal features in the (DA)_n homologue series for $n = 1$ to 4. The transition from dipolar conjugated planar structures (for $n = 1$ and 2) to helicoidal structures (for $n = 3$ and 4) is clearly evidenced by the symmetry-sensitive second-order nonlinear optical experiments. This suggests an approach towards highly efficient chiral chromophores for second-order nonlinear optics. Interestingly, this structural evolution also has significant impact on the photophysical properties: both absorption and fluorescence emission show a bathochromic and hyperchromic shift with increasing number of repeating units in the dipolar planar derivatives ($n = 1-2$) but saturation effect in the helicoidal structures ($n = 2-4$). In addition, the helicoidal structures show sizeable two-photon absorption at 700-750 nm (40-100 GM) for compounds totally lacking either electron-donating or electron-withdrawing substituents.

Keywords

Nonlinear Optics, hyper-Rayleigh scattering, Helicoidal structures, Fluorescence, Two-photon absorption

Introduction

The importance of electron-rich oligothiophenes in general,^[1] and 3,4-ethylenedioxythiophene (EDOT) in particular,^[2] for the design of conjugated materials (including oligomers) with attractive electronic and optical properties, is well recognized.^[3] Among various structures, combining electron-rich aromatic moieties with electron-poor ones, such as pyridine, is a viable strategy to enhance properties that are derived from charge-transfer interaction, relevant for such applications as photovoltaics^[4] and second-order nonlinear optics.^[5] We reported earlier the synthesis of oligomers based on the alternation of electron-poor (pyridyl, A) and electron-rich (3,4-ethylenedioxythienyl, D) heterocycles which show interesting fluorescence properties that strongly depend on their length (Scheme 1).^[6] The optical properties of these chromophores were discussed as a function of their length and their specific electronic and geometrical (coiled structure) features.^[7] One limit to the earlier study being the poor solubility of the oligomers, we here consider more lipophilic derivatives, bearing alkynyl chains at the 4 position of the pyridine rings which allows to expand the series with a longer donor-acceptor DA homologue **4** ($n = 4$, see Scheme 1). To help elucidate the specific relevance of the structural features (in particular the coiled configuration) for the spectroscopic properties, the second-order nonlinear optical (NLO) properties were investigated. The coiled structure in the longer alternated oligomers of these conjugated moieties is an intriguing feature. While for the short homologues, planarity, and hence perfect conjugation over the complete oligomer, is achievable, for the longer homologues, steric hindrance will prevent planarity and will cause breaking of the conjugation towards a helicoidal configuration.^[7] When steric hindrance becomes effective enough, configurational locking allows chiral resolution into the two enantiomers. In this respect, these oligomers are very reminiscent of helicenes.^[8]

Because the lack of mirror symmetry relaxes the stringent symmetry requirements for second-order NLO, chirality has been suggested as a viable approach towards (bulk) noncentrosymmetry.^[9] Chirality has also been used as a crystal engineering tool towards polar crystals of efficient dipolar DA conjugated charge-transfer chromophores, to overcome the strong tendency towards the low-energy centrosymmetric arrangement of such dipoles in aggregates in solution, and in the solid state.^[10] Also, unique contrast patterns in cellular imaging have been obtained from chiral membrane probes derived from the binaphthyl group.^[11]

The critical advantage of our material (series **1-4**) with respect to helicenes is that the EDOT-pyridine building block imparts inherently noncentrosymmetrical DA charge transfer properties in addition to the noncentrosymmetry already derived from the helicoidal configuration. Unsubstituted helicenes exhibit relatively modest second-order NLO properties only derived from the helicoidal configuration,^[8] so that computational and experimental efforts directed towards functionalization of helicenes are needed to increase the nonlinear response.^[12] They also differ from helical polymers on which DA units are grafted to confer second-order NLO activity.^[13] In that case the helicity drives the spatial organization of the NLO-phores^[14] and different strategies are needed to block the helical conformation.^[15]

We report here on a combined synthetic, spectroscopic and computational effort to rationalize the optical properties of soluble alternating EDOT-pyridine oligomers. Apart from the standard spectroscopy tools (linear optics), hyper-Rayleigh scattering (HRS) as a structural symmetry-sensitive probe (second-order NLO) and two-photon excited fluorescence (TPEF, third-order NLO) were determined. Advanced computational techniques were used to underpin the results from symmetry-sensitive second-order NLO experiments. The effect of increasing number of DA repeating units on the photophysical properties (including fluorescence and two-photon absorption properties) is discussed, further evidencing the effect of structural transition from dipolar planar to helicoidal.

Results and discussion

Synthesis

The synthesis of the oligomers **1-4** depicted in Scheme 1 was performed using deprotonation and cross-coupling reactions. The bis-heterocycle **1** was prepared in three steps from 2-chloropyridine (Scheme 2, path a). Treatment with an in situ prepared mixture of 0.5 equiv of ZnCl₂·TMEDA (TMEDA = *N,N,N',N'*-tetramethylethylenediamine) and 1.5 equiv of [Li(tmp)] (tmp = 2,2,6,6-tetramethylpiperidino) in tetrahydrofuran (THF) at room temperature led to metalation at the C-3 and C-4 position in an 83:17 ratio, a result evidenced by subsequent iodine trapping.^[16] The resulting dihalogenopyridine mixture was then reacted with [Li(da)] in THF at -75 °C to allow iodine migration from the 3 to the 4 position.^[17] Under these conditions, the 4-iodo isomer **5a** was isolated in 51% overall yield. As previously documented for similar compounds,^[18] Sonogashira cross-coupling of the heteroaryl iodide **5a** with 1-heptyne selectively and quantitatively afforded the corresponding monocoupled product **6a**. The latter was converted to the bis-heterocycle **1** according to a Negishi-like cross-coupling reaction.^[19] To this purpose, EDOT was converted to the corresponding thienylzinc chloride by deprotonation with butyllithium at 0 °C followed by transmetalation with ZnCl₂·TMEDA. Subsequent reaction with **6a** using a combination of PdCl₂ and 1,1'-

bis(diphenylphosphino)ferrocene (dppf) ligand as the catalyst in refluxing THF gave the bis-heteroaromatic derivative **1** in 88% yield.

In order to progress toward the longer oligomers **2-4**, we considered the synthesis of an analogue of **1**, bearing a chloro group to allow further functionalization. Compound **7** was synthesized in three steps from 2,6-dichloropyridine (Scheme 2, path b). The 4-iodo derivative **5b** was first obtained in 56% yield by metalation/iodination using ^tBuLi and molecular iodine.^[20] It was then converted to **7** through the alkynyl derivative **6b** as described above from **5a**.

The key building block **7** was then used as starting material for the synthesis of **2** using the modified Negishi cross-coupling reaction after deprotonation/transmetalation of **1** (78% overall yield). This strategy was extended with success to the preparation of the elongated alternating oligomers **3-4**. Indeed, using the same cross-coupling method in an iterative synthetic approach and making use of selective deprotonation of the EDOT moiety, heterohexamer **3** and heterooctamer **4** were synthesized in 81-87% yields by coupling **7** with thiophene-deprotonated **2** and **3** respectively (Scheme 3).

Photophysical properties

All photophysical measurements were conducted in chloroform and the corresponding data are collected in Table 1. The data on oligomers (compound **1'-3'**) lacking the alkynyl side chains reported earlier have also been included for comparison purposes.

Linear absorption

The motivation for adding the heptynyl chain was to improve the solubility of the oligomers in organic solvents, in order to include the higher homologue $n = 4$ in the study. Yet this modification was found to induce a consistent red-shift of the low-energy absorption bands as well as of the fluorescence emission. Such bathochromic shift can be related to (hyper)conjugation effect^[21] as well as to slight extension of conjugation due to the presence of the ethynyl linkage. We also note a (non-systematically) varying red-shift in higher-energy absorption bands, and changes in contributions from vibrational progressions. Hence the variation of the absorption maximum values (λ_{max}) is not enough to derive quantitative conclusion. Instead, comparison of the absorption spectra of the different oligomers shows that the low-energy *cut-off* slope in the absorption spectra or the high-energy *cut-on* slope in the emission spectra are shifted by about 20 nm, a value surprisingly valid for all the homologues (see Supporting Information, Figure S11).

In addition to this steady spectral shift observed for all heptynylated homologues, the comparison of the absorption spectra (Figure 1 - left panel) shows that increasing the number of repeating unit (DA) induces bathochromic and hyperchromic effects, indicative of extended electronic conjugation. These

two effects are strongly interlaced in all but the highest-energy band (at 260 nm), resulting in superimpositions and/or shoulders. This is mostly obvious for the shoulders of the low-energy absorption bands of compounds **3** and **4**. Due to these intricacies, it is again informative to consider the low-energy *cut-off* slope in the absorption spectra. A saturation of the *cut-off* values is clearly observed, pointing to a levelling-off in the effective conjugation length for the higher homologues, or alternatively, a distortion of the planarity.

Fluorescence properties

The fluorescence properties are found to depend markedly on the number of DA repeating units, showing a non-monotonous variation: a marked bathochromic shift is observed on going from **1** to **2** while the bathochromic shift is vanishing on going from compound **2** to compound **4**, evidencing a levelling-off of the conjugation in the emissive excited state (Figure 1 - right panel). As observed from the number of DA repeating units also has a major effect on the fluorescence quantum yield. An increase of about one order of magnitude of the fluorescence quantum yield (Φ_f) is observed upon going from **1** (which is only weakly fluorescent) to higher homologues ($\Phi_f = 0.3-0.4$). This effect can be related to both an increase of the radiative decay rate and a decrease of non-radiative rate, in comparison to compound **1**. The much lower radiative decay rate of compound **1**, while its emission is blue-shifted compared to its higher homologues, indicates a much lower transition dipole from the lowest (slightly emissive) excited state to the ground state as compared to higher analogues. Its comparatively much larger non-radiative decay rate also indicates that an efficient non-radiative process competing with fluorescence emission is operating in this compound, suggesting effective intersystem crossing from a singlet to a triplet excited state. This intersystem crossing is consistent with the substantial singlet oxygen generation quantum yield (Φ_A) value determined for compound **1'** ($\Phi_A = 0.47$). Interestingly, the singlet oxygen quantum yield values are observed to further decrease on going from compound **2** ($\Phi_A = 0.35$) to compound **3** and **4** ($\Phi_A = 0.28$ and 0.25). Consistently, a decrease of the non-radiative decay rate is observed on going from compound **2** to **3** or **4**, suggesting a less effective intersystem crossing. In parallel, a continuous slow decrease of the radiative decay rate is observed on going from compound **2** to compound **4**, in relation with the slight red-shift of the emission.^[22] As a result of these combined variations, compound **3** is found to show the largest fluorescence quantum yield ($\Phi_f = 0.4$).

Quite interestingly, while the heptynyl chain was mainly meant to improve solubility of the prepared oligomers, the present study reveals that this side chain significantly affects the photochemical behaviour of the oligomers compounds. In particular, a very interesting feature is the effect of the presence of the heptynyl solubilizing chain on the fluorescence and singlet oxygen quantum yield of the shorter analogues **1** and **2**. In this case, the fluorescence quantum yield is

enhanced by a factor 2 upon ethynylating with respect to the values without alkynyl solubilizing chain (compounds **1'** and **2'**)^[7] while no effect is noted for compound **3** compared to compound **3'**. The larger fluorescence quantum yield of compound **1** compared to its analogue **1'** can be ascribed to a larger radiative rate (whereas the non-radiative rate are similar) suggesting that conjugation extends over the ethynyl moiety in the emitting excited-state of compound **1**, inducing a larger emission transition dipole. In contrast, the larger fluorescence quantum yield of compound **2** compared to compound **2'** can be ascribed to a smaller non-radiative decay rate as in this case the radiative rate are similar, suggesting that the conjugation does extend on the ethynyl moiety in the relaxed excited state in that case). This suggests that the presence of the ethynyl alkyl chain hinders efficient non-radiative decay processes in the case of compound **2**. Such processes could be related either to inter-system crossing (compatible with the much larger singlet oxygen generation quantum yield of compound **2'** compared to compound **2**, resp. 0.85 and 0.35) or to aggregation of compound **2'** favouring competing non-radiative process (such as electron-transfer). Interestingly, compound **3** also show lower singlet oxygen generation quantum yield than his counterpart **3'** lacking the heptynyl chain (resp. 0.56 and 0.28) but the contrast is less marked than in the case of the shorter oligomer **2** and **2'**. Along the same line, we observed that compounds **3** and **3'** show similar quantum yield and lifetimes (as opposed to the case of oligomers **2** and **2'**) and consequently similar radiative and non-radiative rates. Hence the effect of the ethynyl moiety on either aggregation or conjugation in the emissive excited state seems to level off over two repeating units, most probably in relation with the transition from linear to coil structure (vide infra).

Third-order nonlinear optical properties: Two-photon absorption

Thanks to their fluorescence properties, the two-photon absorption properties of compounds **1-4** could be investigated using the well-known protocol based on two-photon excited fluorescence experiments.^[23] Two-photon absorption is a third-order optical process which accordingly does not require absence of centrosymmetry. On the other hand two-photon absorption spectroscopy is of much interest to investigate the various excited state as symmetry rules define one- and two-photon allowed state.^[24] For instance dipolar (or push-pull chromophores) show a lowest excited state which is both one and two-photon allowed while perfect quadrupoles (having a center of symmetry) show one-photon excited state which are two-photon forbidden and conversely two-photon excited state which are not seen under one-photon excitation. In that framework, the investigation of two-photon absorption spectra is of much interest. As seen in Figure 2, compounds **2-4** (i.e. oligomers) show sizeable 2PA response in the spectral range of interest, although they do not bear electron-releasing or electron-withdrawing substituents. Hence the alternation of electron-rich and electron-poor aromatic

units is enough to generate moderate 2PA responses. As observed in Figure 3 showing compared two-photon and (rescaled) one-photon absorption spectra, the lowest excited-state (corresponding to the absorption band in between 800 and 850 nm) is both one- and two-photon allowed. This is consistent with the lack of a centrosymmetry of the molecular structure of all oligomers. We note that the corresponding 2PA responses are rather small (8 to 15 GM) and slightly increases with the number of repeating unit while their position is similar (810-820 nm). On the other hand distinct additional bands are observed at higher energy leading to larger 2PA responses. In particular both oligomers **3** and **4** show a noticeable second maximum located at 750 nm (with corresponding 2PA values of 50 GM) while compound **2** only second maximum located at 720 nm. This second band leading to higher 2PA responses (and similar values for the three compounds) might be related to the specific coiled conformation adopted by oligomers **2-4** (vide infra). Finally all oligomers show even higher 2PA responses at higher energy in connection with a congestion of higher-energy excited states. Compound **4** shows the highest 2PA response at 700 nm (up to 100 GM). Finally oligomer **3** shows the largest two-photon brightness (20 GM) at 750 nm while oligomers **3** and **4** show similar two-photon brightness (30 GM) at 700 nm.

Second-order nonlinear optical properties

The linear optical properties (UV-vis absorption and fluorescence) have a strong influence on the nonlinear optical properties, especially with respect to the laser wavelength dependence and the precision of the obtained results. The first hyperpolarizability β_{HRS} has been determined by hyper-Rayleigh scattering (HRS) at 880 nm (see below). The strong two-photon excited fluorescence (TPEF) contribution to the HRS signal at 440 nm is clear from Figure - left panel, showing the significant low amplitude-modulated (AM) frequency fluorescence contribution to the total HRS signal, in combination with the strong demodulation of this contribution for higher AM frequencies. The substantial TPEF contribution is also evident from the values for the phase lag (Figure - middle panel), approximating values as high as 90° , the maximum value for the phase delay in the case of pure fluorescence, as observed in phase fluorometry.^[25] Also the depolarization ratio (ρ)^[26] measurement is strongly affected by TPEF, as shown in Figure - right panel. This accounts for the rather low precision for the deduced values in presenting the results of the HRS experiments at 880 nm in CHCl_3 . The dynamic first hyperpolarizability values $\beta_{\text{HRS},880}$ (10^{-30} esu) show a very strong increase upon going from the monomer **1** to the tetramer **4**, that does not seem to suffer from saturation. There is, however, a significant effect of resonance enhancement, which becomes more pronounced for the longer structures, as the wavelength of maximal absorption gets closer to the second-harmonic wavelength of 440 nm.

If we apply the simple two-level model^[27] to crudely estimate the effect of the resonance enhancement, the static hyperpolarizability values $\beta_{\text{HRS},0}$ (10^{-30} esu) are obtained. These values show a rather nice linear dependence with number of DA units (within experimental error). The two-level model might imply an oversimplification and involve an overcorrection (due to the closeness of the λ_{max} to the second-harmonic wavelength) for the magnitude of the resonance enhancement factor EF, derived from the λ_{max} for the lowest-energy transition), but this would affect the values in a very gradual way, leaving the finding of the linear dependence of the hyperpolarizability on number of DA units.

It is interesting to observe that both the dynamic and static hyperpolarizability values seem to show a systematic increase with number of DA units, but the ever stronger enhancement of $\beta_{\text{HRS},880}$ for the longer compounds not only results in a very steep slope for $\beta_{\text{HRS},880}$ as a function of n , but particularly in a negative intercept for the dynamic $\beta_{\text{HRS},880}$ values (at the mathematically relevant $n = 0$), while the linear dependence for the static $\beta_{\text{HRS},0}$ values after correction for resonance enhancement results in a physically much more acceptable zero intercept ($-7 \pm 14 \times 10^{-30}$ esu for $n = 0$) and, much more physically relevant, a constant slope of $(30 \pm 5) \times 10^{-30}$ esu per DA unit. Especially the zero intercept lends additional credibility to the resonance correction.

It might be correctly argued that this two-level model is oversimplified. However, from the complexity of the absorption spectrum, it was deemed overambitious to attempt a more complete analysis of the contributions from the different bands to the second-order NLO response. Irrespective of the interpretation of the hyperpolarizability values in terms of resonance or not, the general conclusion from the hyperpolarizability measurements should be that there is a linear increase going from **1** to **4** without any sign of saturation. It is highly instructive to also review the other parameters in Table 2 that could be deduced from the analysis. The retrieved fluorescence lifetime τ found here is confirming the trend of longer lifetimes reported in Table 1. There is no quantitative agreement, as the experimental conditions are quite different (880 nm TPEF at 440 nm as a side effect in HRS, versus dedicated experimental setup with one-photon excitation and detection at emission maximum). The robustness of the hyperpolarizability results against detailed fluorescence decay profile has been demonstrated earlier.^[28]

More importantly, the TPEF contribution, revealed as its amplitude at 1 kHz AM frequency, A_{TPEF} , is confirming the earlier observations about the third-order nonlinear optical properties: Also in this TPEF contribution, we see a negligible contribution for **1**, and an almost linear increase for **2**, **3** and **4**.

To gain more insight in the symmetry of the chromophores, and the nature of the second-order nonlinear response, the HRS depolarization ρ values were estimated.^[26] Because of the significant

TPEF contribution, ρ values were seriously underestimated, inherently at 1 kHz because of the strong fluorescence depolarization at low AM frequency, but still at the highest AM frequency of 880 MHz. We had to resort to simultaneous fitting of all observables to arrive at still rather crude estimates for the fluorescence-free ρ values^[8] is providing the 3 sets of ρ values.

Theoretical results

Geometry optimizations were performed on the successive oligomers where the C_5H_{11} groups are replaced by CH_3 groups and where the starting conformations match the X-ray diffraction data of reference^[7]. They show that for $n = 1-3$ the systems are mostly planar whereas from $n = 4$ a helix starts to form in order to avoid steric hindrance (Figure 5). Additional calculations demonstrate that linear oligomers obtained by a π -rotation of the dihedral angles between the pyridine and EDOT rings are less stable. The calculated first hyperpolarizability values are listed in Table 3 and presented in Figure . The HRS value β_{HRS} increases almost linearly for n ranging between 1 and 4 and then it levels off. The corresponding depolarization ratio ρ is close to the value of 1.5, typical of octupolar systems, when $n = 3-5$ whereas for smaller system a more dipolar character is observed. The EFISHG data are different and show oscillations in the $\beta_{//}$ values as a function of n . $\beta_{//}$ is maximum for $n = 2$, then decreases and increases again.

Analysis and effect of conformational transition

The linear optical properties, and also the third-order nonlinear optical properties can to a large extent be analyzed in terms of number of EDOT and pyridine units, or, conversely, in terms of conjugation length. There is a clear influence of the number of units on the oscillator strength of the highest-energy transition at about 260 nm. This influence becomes less obvious in the lower-energy bands, where there is a considerable red-shift of the bands observed. This red-shift of multiple bands is causing the lowest-energy band to end up as a mere shoulder (at 422 nm) for compound **4**, while it is still observable as a local maximum at 415 nm for compound **3**. The red-shift is indicative of increased conjugation length, so the saturation in red-shift points to an effective conjugation length not growing with the number of conjugated units when $n > 3$, or to an increasing distortion away from planarity. From linear optics (and by the same token, from third-order nonlinear optics) nothing more can be indisputably derived, since odd-order effects are not symmetry-sensitive, or more precisely do not require lack of centrosymmetry.

This is where second-order nonlinear optical properties can provide more specific insight, since even-order effects are critically sensitive to symmetry. We observe that the first

hyperpolarizability (second-order nonlinear optical molecular polarizability) is increasing linearly with the number of units for $n = 1-4$. More instructively, the depolarization ratio ρ shows that the shorter compounds behave largely as a dipolar chromophore, but that the longer compounds do not continue to extend along a single major molecular dipolar axis. This is most explicitly demonstrated in the theoretically derived $\beta_{J=1}$ and $\beta_{J=3}$ values (Figure). At $n = 1$, $\beta_{J=1} > \beta_{J=3}$ so that NLA is smaller than 1 but from $n = 1$ to 4, the octupolar $\beta_{J=3}$ contribution increases linearly while the dipolar $\beta_{J=1}$ contribution decreases. So, the octupolar contribution becomes dominant and dictates the evolution of β_{HRS} with n . Going from $n = 4$ to 5, the octupolar contribution saturates and the dipolar one increases so that NLA decreases. The transition from dominant dipolar ($n = 1$) to octupolar ($n = 2-5$) response is also visible when analyzing the β_{\parallel} EFISH response but the θ angle between the dipole moment and the vector part of β plays also a role. Indeed, for $n = 1$ to 5, $\theta = 60^\circ, 22^\circ, 33^\circ, 31^\circ$, and 33° , respectively. Both analyses nicely corroborate the lower depolarization ratios for **3** and **4** indeed, pointing to a non-dipolar symmetry.

Finally, reverting to the observed changes in fluorescence quantum yield, it is conjectured that the effects of higher homologues and that of alkynylating are orthonormal in preventing self-aggregation and quenching, either through the increased solubility by the chain, or by the deviation from planarity. The lowest fluorescence quantum yield is observed for non-alkynylated DA $n = 1$,^[7] where the lower solubility and the planarity both are ideally conducive towards aggregation and quenching (leading both to the lowest radiative rate and higher non-radiative rate). Either alkynylation (increase by factor of 2) or oligomerization (**1** to **3**) results in a quantum yield of over 30%. This value is obtained already for compound **2**, which combines both structural features of coiling and solubilizing. In the DA series without solubilizing tail, the higher fluorescence quantum yield is only obtained for (DA)₃,^[7] which then has the stronger deviation from planarity, in agreement with the rationale derived from depolarization ratios. An alternative explanation can be in terms of reduced torsional degrees of freedom as a consequence of the intramolecular H-bridges and repulsion between the N and O atoms of successive rings, also effects that become more pronounced for higher homologues (longer oligomers), but this could not explain the effect of alkynylation.

Interestingly the transition from linear to coiled structure is also apparent in the onset of the 2PA band at higher energy (720-750 nm) to sizeable 2PA response (40-50 GM) for chromophores which totally lack either electron-donating or electron-withdrawing substituents.

Conclusions and Perspectives

From an integrated synthetic, spectroscopic and computational approach, we have been able to rationalize the linear and nonlinear optical properties of a homologue series of alternated EDOT-alkynylpyridine oligomers in terms of an increasingly non-planar non-dipolar, coiled structure with a limiting effective conjugation length. For the shorter (DA)_n n = **1** or **2** homologues, a largely dipolar response from unsaturated and planar effective conjugation is observed, while for the n = **2**, **3** and **4** homologues, increasingly non-dipolar/octupolar response is attributed to the coiled structures with deviation from planarity. The dipolar part of the second-order nonlinear optical response is shown to follow this argumentation, while the total second-order nonlinear optical response is not levelling off for the higher homologues. This confirms the unique features of coiled molecular structures for second-order nonlinear optical properties.

In ensembles of molecules, or in thin film solid state format for practical applications in second-order nonlinear optics, the non-centrosymmetry should be conserved at this supramolecular level. To this end, resolution of the helicoidal structures in the two chiral enantiomers should be attempted. It is expected that **3** is still configurationally unstable,^[7] but steric hindrance in **4** should be sufficient to lock the helical structure for chiral resolution. Alternatively, introducing more steric hindrance in shorter oligomers has been shown to be an effective resolution strategy in pentahelquats.^[29]

Finally, synthetic efforts towards even higher, yet still soluble, homologues could lead towards configurationally stable and even more efficient optical materials, since experimentally, no saturation of the second- and third-order nonlinear optical properties has yet been observed, although the computational result seems to suggest the onset of clamping of the HRS hyperpolarizability.

Acknowledgements

We are grateful to the Université de Rennes 1 and the CNRS for support (F.C. and F.M.). MBD acknowledges financial support from Rennes Metropole and stimulating discussion with Olivier Mongin. This work is supported by funds from the Francqui Foundation. The calculations were performed on the computers of the Consortium des Équipements de Calcul Intensif and mostly those of the Technological Platform of High-Performance Computing, for which we gratefully acknowledge the financial support of the FNRS-FRFC (Conventions No. 2.4.617.07.F and 2.5020.11) and of the University of Namur.

Experimental Section

Synthesis

The reactions were performed in Schlenk tubes under an argon atmosphere. THF was freshly distilled over sodium/benzophenone. Commercially available starting materials were used without further purification. Liquid chromatography separations were achieved on silica gel Merck-Geduran Si 60 (63-200 μm). Nuclear magnetic resonance (NMR) spectra were acquired on Bruker AC-300 (300 and 75 MHz for ^1H and ^{13}C , respectively) spectrometer. ^1H chemical shifts (δ) are given in ppm relative to the solvent residual peak and ^{13}C chemical shifts relative to the central peak of the solvent signal.^[30] Coupling constants (J) are given in Hz. High-resolution mass spectra measurements were performed at the Centre Régional de Mesures Physiques de l'Ouest (CRMPO) in Rennes.

2-Chloro-4-iodopyridine (5a). To a stirred, cooled (0 °C) solution of 2,2,6,6-tetramethylpiperidine (1.0 mL, 6.0 mmol) in THF (10 mL) were successively added $n\text{BuLi}$ (1.6 M hexanes solution, 6.0 mmol) and $\text{ZnCl}_2\cdot\text{TMEDA}$ (0.51 g, 2.0 mmol). The mixture was stirred for 15 min at 0 °C before introduction of 2-chloropyridine (0.45 g, 4.0 mmol). After 2 h at room temperature, a solution of I_2 (1.5 g, 6.0 mmol) in THF (10 mL) was added. The mixture was stirred overnight before addition of an aqueous saturated solution of $\text{Na}_2\text{S}_2\text{O}_3$ (40 mL) and extraction with CH_2Cl_2 (3 \times 40 mL). The combined organic layers were dried over Na_2SO_4 , filtered and concentrated under reduced pressure. The crude product was directly used in the next step. To a stirred, cooled (-75 °C) solution $n\text{BuLi}$ (1.6 M hexanes solution, 4.0 mmol) in THF (30 mL) were successively added diisopropylamine (0.41 g, 4.0 mmol) and the crude mixture. The mixture was stirred for 4 h at -75 °C before addition of water (50 mL) and extraction with diethyl ether (3 \times 50 mL). The combined organic layers were dried over MgSO_4 , filtered and concentrated under reduced pressure. Purification by flash chromatography on silica gel (heptane/ CH_2Cl_2 : 4/1) gave **5a** (488 mg, 51%) as a white solid (mp 40 °C). ^1H NMR (CDCl_3 , 300 MHz) 7.58 (dd, 1H, $J = 1.4$ and 5.2), 7.74 (dd, 1H, $J = 0.5$ and 1.4), 8.06 (dd, 1H, $J = 0.4$ and 5.2). ^{13}C NMR (CDCl_3 , 75 MHz) 106.7, 131.7, 133.2, 149.8, 151.9. These values are consistent with the literature.^[17]

2,6-Dichloro-4-iodopyridine (5b). To a stirred, cooled (-75 °C) solution of 2,6-dichloropyridine (4.4 g, 30 mmol) in THF (50 mL) was added $n\text{BuLi}$ (1.6 M hexanes solution, 30 mmol). After 45 min at -75 °C, a solution of I_2 (7.6 g, 30 mmol) in THF (20 mL) was added. The mixture was stirred 15 min before addition of an aqueous saturated solution of $\text{Na}_2\text{S}_2\text{O}_3$ (25 mL) and extraction with Et_2O (3 \times 20 mL). The combined organic layers were dried over MgSO_4 , filtered and concentrated under reduced pressure. Precipitation in AcOEt gave **5b** (4.6 g, 56%) a white powder

(mp 160 °C). ^1H NMR (CDCl_3 , 300 MHz) 7.65 (s, 2H). ^{13}C NMR (CDCl_3 , 75 MHz) 107.8, 131.6 (2C), 150.7 (2C). These values are consistent with the literature.^[20]

2-Chloro-4-(1-heptynyl)pyridine (6a). To a stirred solution of **5a** (3.6 g, 15 mmol) in degassed THF (200 mL) were successively added 1-heptyne (1.6 g, 16 mmol), diethylamine (5.5 g, 76 mmol), CuI (0.29 g, 10 mol%) and $\text{PdCl}_2(\text{PPh}_3)_2$ (0.53 g, 5 mol%) at room temperature. The reaction mixture was stirred for 12 h at room temperature, quenched with water (1 mL) and filtered over celite[®]. Purification by flash chromatography on silica gel (heptane/ CH_2Cl_2 : 4/1) gave **6a** (3.0 g, 98%) as a yellow oil. ^1H NMR (CDCl_3 , 300 MHz) 0.92 (t, 3H, $J = 7.0$), 1.33-1.63 (m, 6H), 2.41 (t, 2H, $J = 7.1$), 7.15 (dd, 1H, $J = 1.3$ and 5.1), 7.29 (br s, 1H), 8.28 (dd, 1H, $J = 0.7$ and 5.1). ^{13}C NMR (CDCl_3 , 75 MHz) 14.0, 19.5, 22.2, 28.0, 31.1, 77.5, 97.9, 124.5, 126.3, 135.3, 149.4, 151.6. HRMS (ESI): calcd for $\text{C}_{12}\text{H}_{15}\text{ClN}$ $[\text{M}+\text{H}]^+$ 208.0893, found 208.0892.

2,6-Dichloro-4-(1-heptynyl)pyridine (6b). The above described procedure used for **6a** was employed starting from **5b** (4.1 g, 15.0 mmol), THF (200 mL), 1-heptyne (1.6 g, 16 mmol), diethylamine (5.5 g, 76 mmol), CuI (0.29 g, 10 mol%) and $\text{PdCl}_2(\text{PPh}_3)_2$ (0.53 g, 5 mol%). Purification by flash chromatography on silica gel (heptane/ CH_2Cl_2 : 1/1) gave **6b** (3.6 g, 99%) as a yellow oil. ^1H NMR (CDCl_3 , 300 MHz) 0.92 (t, 3H, $J = 7.0$), 1.33-1.62 (m, 6H), 2.42 (t, 2H, $J = 7.1$), 7.20 (s, 2H). ^{13}C NMR (CDCl_3 , 75 MHz) 14.1, 19.6, 22.3, 28.0, 31.2, 76.7, 99.6, 124.9 (2C), 137.5, 150.6 (2C). HRMS (ESI): calcd for $\text{C}_{12}\text{H}_{14}\text{Cl}_2\text{N}$ $[\text{M}+\text{H}]^+$ 242.05033, found 242.0502.

2-(3,4-Ethylenedioxy-2-thienyl)-4-(1-heptynyl)pyridine (1). To a stirred, cooled (-78 °C) solution of EDOT (0.43 g, 3.0 mmol) in dry THF (5 mL) was slowly added $n\text{BuLi}$ (1.6 M hexanes solution, 3.0 mmol). After introduction of $\text{ZnCl}_2\cdot\text{TMEDA}$ (0.76 g, 3.0 mmol), the temperature was raised to 0 °C. The mixture was stirred for 1 h at 0 °C and PdCl_2 (11 mg, 2 mol%), dppf (33 mg, 2 mol%) and **6a** (0.62 g, 3.0 mmol) were successively added. The reaction mixture was stirred for 48 h at 60 °C, quenched with water (1 mL) and filtered over celite[®]. After addition of an aqueous saturated solution of NaCl (10 mL), the mixture was extracted with CH_2Cl_2 (3 x 10 mL). The combined organic layers were dried over MgSO_4 , filtered and concentrated under reduced pressure. Purification by flash chromatography on silica gel (heptane/ CH_2Cl_2 : 3/2) gave **1** (827 mg, 88%) as a yellow solid (mp 65 °C). ^1H NMR (CDCl_3 , 300 MHz) 0.91 (t, 3H, $J = 7.0$), 1.35-1.64 (m, 6H), 2.41 (t, 2H, $J = 7.1$), 4.21-4.36 (m, 4H), 6.42 (s, 1H), 7.01 (dd, 1H, $J = 1.5$ and 5.1), 7.89 (br s, 1H), 8.40 (dd, 1H, $J = 0.9$ and 5.1). ^{13}C NMR (CDCl_3 , 75 MHz) 14.1, 19.6, 22.3, 28.2, 31.2, 64.4, 65.1, 79.0, 95.5, 101.6, 118.4, 122.3, 123.1, 132.7, 140.2, 142.1, 149.0, 151.6. HRMS (ESI): calcd for $\text{C}_{18}\text{H}_{19}\text{NO}_2\text{S}$ $[\text{M}+\text{H}]^+$ 336.1034, found 336.1047.

2-Chloro-6-(3,4-ethylenedioxy-2-thienyl)-4-(1-heptynyl)pyridine (7). The above described procedure used for **1** was employed starting from EDOT (0.43 g, 3.0 mmol), THF (5 mL), $n\text{BuLi}$ (1.6

M hexanes solution, 3.0 mmol), ZnCl₂·TMEDA (0.76 g, 3.0 mmol), PdCl₂ (11 mg, 2 mol%), dppf (33 mg, 2 mol%) and **6b** (0.73 g, 3.0 mmol). Purification by flash chromatography on silica gel (heptane/CH₂Cl₂: 6/4) gave **7** (0.76 g, 73%) as a yellow solid (mp 90 °C). ¹H NMR (CDCl₃, 300 MHz) 0.92 (t, 3H, *J* = 7.0), 1.31-1.64 (m, 6H), 2.42 (t, 2H, *J* = 7.1), 4.22-4.38 (m, 4H), 6.45 (s, 1H), 7.04 (d, 1H, *J* = 1.1), 7.78 (d, 1H, *J* = 1.1). ¹³C NMR (CDCl₃, 75 MHz) 14.1, 19.6, 22.3, 28.1, 31.2, 64.4, 65.2, 78.1, 96.9, 102.8, 117.1, 120.7, 123.0, 132.5, 140.9, 142.0, 150.6, 152.0. HRMS (ESI): calcd for C₁₈H₁₉ClNO₂S [M+H]⁺ 348.0825, found 348.0834.

2-(6-(3,4-Ethylenedioxy-2-thienyl)-4-(1-heptynyl)-2-pyridyl)-5-(4-(1-heptynyl)-2-pyridyl)-3,4-ethylenedioxythiophene (2). The above described procedure used for **1** was employed starting from **1** (0.94 g, 3.0 mmol), ⁿBuLi (1.6 M hexanes solution, 3.0 mmol), ZnCl₂·TMEDA (0.76 g, 3.0 mmol), PdCl₂ (11 mg, 2 mol%), dppf (33 mg, 2 mol%), **7** (1.0 g, 3.0 mmol) and THF (5 mL). Purification by flash chromatography on silica gel (heptane/CH₂Cl₂: 4/1) gave **2** (1.46 g, 78%) as a yellow solid (mp 128 °C). ¹H NMR (CDCl₃, 300 MHz) 0.93 (br t, 6H, *J* = 7.0), 1.42 (m, 8H), 1.65 (m, 4H), 2.43 (t, 2H, *J* = 7.1), 2.44 (t, 2H, *J* = 7.1), 4.24 (m, 2H), 4.36 (m, 2H), 4.43 (s, 4H), 6.43 (s, 1H), 7.04 (dd, 1H, *J* = 1.5 and 5.1), 7.70 and 7.72 (AB, d, 2H, *J* = 1.2), 7.93 (br s, 1H), 8.49 (dd, 1H, *J* = 0.8 and 5.1). ¹³C NMR (CDCl₃, 75 MHz) 14.1, 14.2, 19.6, 19.7, 22.3, 22.4, 28.3, 28.4, 31.3, 31.4, 64.5, 64.8, 64.9, 65.1, 79.1, 79.5, 94.7, 95.5, 102.2, 119.0, 119.9, 120.0, 120.3, 120.4, 123.1, 123.4, 132.6, 132.9, 140.0, 140.1, 140.2, 141.9, 149.2, 150.5, 150.9, 151.7. HRMS (ESI): calcd for C₃₆H₃₇N₂O₄S₂ [M+H]⁺ 625.2195, found 625.2198.

2-[6-[5-(4-(1-Heptynyl)-2-pyridyl)-3,4-ethylenedioxy-2-thienyl]-4-(1-heptynyl)-2-pyridyl]-5-[6-(3,4-ethylenedioxy-2-thienyl)-4-(1-heptynyl)-2-pyridyl]-3,4-ethylenedioxythiophene (3). The above described procedure used for **1** was employed starting from **2** (0.63 g, 1.0 mmol), ⁿBuLi (1.6 M hexanes solution, 1.0 mmol), ZnCl₂·TMEDA (0.25 g, 1.0 mmol), PdCl₂ (4 mg, 2 mol%), dppf (11 mg, 2 mol%), **7** (0.35 g, 1.0 mmol) and THF (5 mL). Purification by flash chromatography on silica gel (heptane/CH₂Cl₂: 7/3) gave **3** (758 mg, 81%) as a yellow solid (mp 146 °C). ¹H NMR (CDCl₃, 300 MHz) 0.94 (m, 9H), 1.34-1.71 (m, 18H), 2.45 (m, 6H), 4.25 (m, 2H), 4.43 (m, 10H), 6.45 (s, 1H), 7.05 (dd, 1H, *J* = 1.3 and 5.1), 7.66 and 7.69 (AB, d, 2H, *J* = 1.2), 7.72 and 7.73 (AB, d, 2H, *J* = 1.3), 7.91 (dd, 1H, *J* = 0.9 and 1.3), 8.47 (dd, 1H, *J* = 0.9 and 5.1). ¹³C NMR (CDCl₃, 75 MHz) 14.1, 14.2 (2C), 19.6, 19.7 (2C), 22.3, 22.4 (2C), 28.3, 28.4 (2C), 31.3, 31.4 (2C), 64.6, 64.8 (2C), 64.9 (2C), 65.2, 79.1, 79.6 (2C), 94.6, 94.7, 95.4, 102.0, 118.9, 119.8, 120.0, 120.2, 120.3, 120.4, 120.6, 120.7, 120.8, 123.0, 123.3, 132.5, 132.8, 132.9, 139.9, 140.0, 140.1, 140.2, 140.3, 141.9, 149.1, 150.7, 150.8, 150.9, 151.0, 151.8. HRMS (ESI): calcd for C₅₄H₅₄N₃O₆S₃ [M+H]⁺ 936.3175, found 936.3165.

2-[6-[5-[6-(3,4-Ethylenedioxy-2-thienyl)-4-(1-heptynyl)-2-pyridyl]-3,4-ethylenedioxy-2-thienyl]-4-(1-heptynyl)-2-pyridyl]-5-[6-[5-(4-(1-heptynyl)-2-pyridyl)-3,4-ethylenedioxy-2-

thienyl]-4-(1-heptynyl)-2-pyridyl]-3,4-ethylenedioxythiophene (4). The above described procedure used for **1** was employed starting from **3** (0.94 g, 1.0 mmol), ^tBuLi (1.6 M hexanes solution, 1.0 mmol), ZnCl₂·TMEDA (0.25 g, 1.0 mmol), PdCl₂ (4 mg, 2 mol%), dppf (11 mg, 2 mol%), **7** (0.35 g, 1.0 mmol) and THF (5 mL). Purification by flash chromatography on silica gel (heptane/CH₂Cl₂: 7/3) gave **4** (1.09 g, 87%) as a yellow solid (mp 182 °C). ¹H NMR (CDCl₃, 300 MHz) 0.95 (m, 12H), 1.35-1.69 (m, 24H), 2.45 (m, 8H), 4.16-4.60 (m, 16H), 6.11 (s, 1H), 6.91 (dd, 1H, *J* = 1.2 and 5.0), 7.58-7.74 (m, 6H), 7.80 (br s, 1H), 8.21 (d, 1H, *J* = 5.0). ¹³C NMR (CDCl₃, 75 MHz) 14.1 (4C), 19.6, 19.7 (3C), 22.3, 22.4 (3C), 28.4 (4C), 31.3, 31.4 (3C), 64.4, 64.9 (4C), 65.0 (3C), 79.3, 79.5, 79.6, 79.7, 94.3, 94.5, 94.6, 94.9, 102.3, 118.9, 119.6-120.7 (12C), 122.8, 123.0, 131.9, 132.7, 132.8 (2C), 139.7, 140.0, 140.1, 140.2, 140.3, 140.4, 140.6, 141.3, 148.8, 150.6, 150.7, 150.8, 150.9, 151.0, 151.3, 151.5. HRMS (ESI): calcd for C₇₂H₇₁N₄O₈S₄ [M+H]⁺ 1247.41548, found 1247.4173.

Photophysical studies

All photophysical properties have been performed with freshly-prepared solutions of the chromophores in air-equilibrated toluene at room temperature (298 K). UV/Vis absorption spectra were recorded on a Jasco V-570 spectrophotometer. Steady-state and time-resolved fluorescence measurements were performed on dilute solutions (*ca.* 10⁻⁶ M, optical density < 0.1) contained in standard 1 cm quartz cuvettes using an Edinburgh Instruments (FLS920) spectrometer in photon-counting mode. Emission spectra were obtained, for each compound, under excitation at the wavelength of the absorption maximum. Fluorescence quantum yields were measured according to literature procedures using quinine in 0.5 M H₂SO₄ as a standard (quantum yield Φ_f = 0.55).^[31] The reported fluorescence quantum yields are within ±10%. The fluorescence lifetime values were obtained from the reconvolution fit analysis (Edinburgh F900 analysis software) of decay profiles obtained using the FLS920 instrument under excitation with a nitrogen-filled nanosecond flashlamp. The quality of the fits was evidenced by the reduced χ² value (χ² < 1.1). Measurements of singlet oxygen quantum yield (Φ_Δ) were performed on a Fluorolog-3 (Horiba Jobin Yvon), using a 450 W Xenon lamp. The emission at 1272 nm was detected using a liquid nitrogen-cooled Ge-detector model (EO-817L, North Coast Scientific Co). Singlet oxygen quantum yields Φ_Δ were determined in chloroform solutions, using tetraphenylporphyrin (TPP) in chloroform as reference solution (Φ_Δ = 0.55) and were estimated from ¹O₂ luminescence at 1272 nm.

Third-order nonlinear optical method: two-photon excited fluorescence measurements

Two-photon excitation cross-sections (σ₂) of chromophores **1-4** were determined by investigating their two-photon-excited fluorescence (TPEF) in solution. These measurements provide

the TPEF action cross-section $\sigma_2\Phi_f$. The corresponding σ_2 values were derived by determining the fluorescence quantum yield Φ_f from standard fluorescence measurements (vide supra). TPEF measurements were conducted using a mode-locked Ti:sapphire laser operating between 700 and 1000 nm and delivering 80 fs pulses at 80 MHz, using the well-established method described by Xu and Webb,^[23a] and the appropriate solvent-related refractive index corrections.^[23a] The quadratic dependence of the fluorescence intensity on the excitation intensity was verified for each data point, indicating that the measurements were carried out in intensity regimes, in which saturation or photodegradation do not occur. TPEF measurements were calibrated relative to the absolute TPEF action cross-section determined by Xu and Webb for fluorescein in 0.01M aqueous NaOH for 700-980 nm.^[23a] The experimental uncertainty amounts to $\pm 10\%$.

Second-order nonlinear optical method: hyper-Rayleigh scattering

As a more widely applicable characterization method for second-order nonlinear optical properties at the molecular level, hyper-Rayleigh scattering (HRS) has been used.^[32] This method provides two experimental observables, the total HRS scattering intensity, which can be related to the tensor component averaged $\beta_{\text{HRS}}(-2\omega;\omega,\omega)$, and the HRS depolarization ratio (ρ), which can provide information about the molecular symmetry.

Based on the linear optical properties (UV-vis absorption spectra), it was decided to perform HRS experiments at 880 nm, as a compromise between resonance enhancement and absorption of the HRS signal at the second harmonic wavelength of 440 nm. The other rationale, for not shifting to even longer fundamental wavelengths, is to make use of the high power of a Titanium-sapphire femtosecond laser (a longer wavelength implies a serious drop of power from the Titanium-sapphire laser, or the use of an optical parametric oscillator pumped by this Titanium-sapphire laser, in either case a serious reduction of laser power).

Because of the fluorescent properties of the chromophores, it was imperative to use amplitude-modulated (AM) frequency-resolved femtosecond hyper Rayleigh scattering.^[33] A two-photon excited fluorescence (TPEF) contribution to the HRS signal at low AM frequency (chopper frequency of 1 kHz) at 440 nm was observed for all samples. At the higher AM frequencies (up to 880 MHz) the TPEF contribution was almost completely demodulated and the phase shift between immediate nonlinear scattering for a non-fluorescent reference and the fluorescent samples had passed its maximum.^[34] From the simultaneous data analysis of modulus and phase of the HRS signal as a function of AM frequency towards the TPEF contribution at 1 kHz, the fluorescence lifetime and the first hyperpolarizability, an accurate and fluorescence-free hyperpolarizability can be extrapolated for the high AM frequency limit. This approach in the frequency domain is our Fourier-transform implementation of the discrimination between scattering and fluorescence in the time domain. The

AM frequency components are obtained as the inherent harmonic content of the femtosecond laser pulse with a repetition frequency of 80 MHz for the Titanium sapphire laser (model Tsunami, Spectra-Physics).^[33]

To gain more insight in the molecular symmetry, or the nature of the second-order NLO response, depolarization ratios (ρ) were also experimentally determined.^[26] However, due to the TPEF contribution, this ρ had also to be determined as a function of AM frequency, since the TPEF contribution is strongly depolarized, resulting in a ρ of 1.0 at 1kHz, and only going up to physically relevant values for HRS ρ for the higher AM frequencies.^[8] To obtain reliable experimental values for the ρ , a simultaneous fitting of modulus, phase and ρ was implemented. For the ρ as a function of AM frequency, this analysis results in the low-frequency ρ value (depolarized because of the fluorescence depolarization) and the high-frequency ρ value, without fluorescence effects, hence the true HRS ρ .

Because of the substantial TPEF contribution to both HRS total signal and ρ at low AM frequencies, the extrapolation at high AM frequencies towards TPEF-free β_{HRS} and ρ yields accurate values, yet with rather low precision.

Theoretical and computational methods

The ground state geometries were optimized at the density functional theory (DFT) level of approximation by employing the B97-D exchange-correlation (XC) functional and the 6-311G(d) basis set. The B97-D XC functional includes semi-empirical dispersion corrections and is therefore well-suited to account for the London dispersion forces between the successive helix turns.^[35] Neglecting these interactions would indeed lead to an overestimated helical pitch as that was obtained for pyridine-pyrimidine helical oligomers when using the standard B3LYP XC functional as well as the AM1, PM3, or PM5 semi-empirical schemes.^[13]

The time-dependent DFT (TDDFT) method was adopted to calculate the first hyperpolarizabilities, in combination with the long-range corrected LC-BLYP XC functional^[36] (with a range-separating parameter $\mu = 0.47$) and the 6-311+G(d) basis set. In the LC-BLYP treatment, the electron repulsion operator and thereof the exchange (X) is partitioned using the error function into short- and long-range parts. The short-range part modifies a conventional DFT exchange potential (here the Becke functional), while the long-range part is inserted into the Hartree-Fock exchange expression.^[37] This functional enables to avoid the chain-length-dependent overpolarization that is characteristic of conventional X functionals^[38] and that has been traced back to their short-sightedness.^[39] Owing to recent contrasted results for calculating β of extended systems,^[40] the standard range-separated parameter ($\mu = 0.47$) was used rather than a physically-motivated value

determined to reproduce Koopmans' theorem.^[39] Time-dependent Hartree-Fock (TDHF) calculations were also performed and are consistent with the TDDFT/LC-BLYP results (SI).

The effects of the solvent were accounted for using the polarizable continuum model within the integral equation formalism (IEF-PCM),^[41] where the solvent is approximated as a structureless polarizable continuum characterized by its macroscopic dielectric permittivity. Dichloromethane was used as solvent ($n = \epsilon_\infty = 2.03$). The calculations were done at 1064 nm, which using the LC-BLYP XC functional can still be considered essentially "off-resonance", or for any practical comparative purposes within this series, with very small resonance enhancement. The choice of a dynamic dielectric constant enables to avoid the large static dielectric constant ϵ_0 of the solvent that would overestimate the solvent effects on β and therefore to get close to the experiment situation where measurements are performed at optical wavelengths and then extrapolated to infinite wavelength.

Starting from the 18 independent $\beta(-2\omega; \omega, \omega)$ tensor components, two measured quantities have been calculated, *i.e.* i) the $\beta_{\text{HRS}}(-2\omega; \omega, \omega)$ hyper-Rayleigh scattering (HRS) response that is related to the HRS intensity for plane-polarized incident light and observation made perpendicularly to the propagation direction,

$$b_{\text{HRS}}(-2\omega; \omega, \omega) = \sqrt{\langle b_{\text{ZZZ}}^2 \rangle + \langle b_{\text{ZXX}}^2 \rangle} \quad (1)$$

and ii) its depolarization ratio (ρ) that corresponds to the intensity ratio for measurements performed in the VV (vertically polarized incident and scattered lights) and HV (horizontally polarized incident light and vertically polarized scattered light) configurations, respectively

$$\rho = \frac{I_{\text{VV}}^{2\omega}}{I_{\text{HV}}^{2\omega}} = \frac{\langle \beta_{\text{ZZZ}}^2 \rangle}{\langle \beta_{\text{ZXX}}^2 \rangle} \quad (2)$$

where the full expressions for $\langle b_{\text{ZZZ}}^2 \rangle$ and $\langle b_{\text{ZXX}}^2 \rangle$, quadratic products of β tensor components, which correspond to isotropic averaging over the molecular motions, can be found in several textbooks and publications.^[5a, 42] Calculated β was also decomposed into its dipolar ($J = 1$) and octupolar ($J = 3$) tensorial components, which are related to the quadratic averages. Assuming Kleinman's conditions,

$$\langle b_{\text{ZZZ}}^2 \rangle = \frac{9}{45} |b_{J=1}|^2 + \frac{6}{105} |b_{J=3}|^2 \quad (3)$$

$$\langle b_{\text{ZXX}}^2 \rangle = \frac{1}{45} |b_{J=1}|^2 + \frac{4}{105} |b_{J=3}|^2 \quad (4)$$

The nonlinear anisotropy parameter $NLA = \left| \frac{b_{j=3}}{b_{j=1}} \right|$ compares the relative contributions of the octupolar and dipolar components to the first hyperpolarizability tensor β while it is linked to the depolarization ratio. The extreme cases correspond to fully octupolar and dipolar responses and their NLA values amount to ∞ and 0 ($\rho = 3/2$ and 9) whereas for a one-dimensional push-pull system with a unique dominant diagonal β tensor component, $NLA = 0.82$ ($\rho = 5$), respectively. In addition the $\beta_{//}(-2\omega; \omega, \omega)$ quantity has been calculated, which can be deduced from electric field-induced second-harmonic generation (EFISHG) measurements, and that corresponds to the projection of the vector part of β on the dipole moment vector:

$$b_{//}(-2\omega; \omega, \omega) = b_{//} = \frac{1}{5} \dot{\mathbf{a}}_i \frac{m_i}{\|m\|} \dot{\mathbf{a}}_j (b_{ijj} + b_{jij} + b_{jji}) = \frac{3}{5} \dot{\mathbf{a}}_i \frac{m_i b_i}{\|m\|} \quad (5)$$

where $\|m\|$ is the norm of the dipole moment, μ_i and β_i are the components of the μ and β vectors. All β values are given within the B convention. All calculations were performed using Gaussian09.^[43]

References

- [1] a) T.-G. Zhang, Y. Zhao, I. Asselberghs, A. Persoons, K. Clays, M. J. Therien, *J. Am. Chem. Soc.* **2005**, *127*, 9710-9720; b) S. M. Bouzzine, M. Hamidi, M. Bouachrine, F. Serien-Spirau, J. P. Lere Porte, J. M. Sotiropoulos, A. Iraqi, *J. Phys. Chem. A* **2012**, *116*, 9730-9738.
- [2] a) J. Roncali, P. Blanchard, P. Frère, *J. Mater. Chem.* **2005**, *15*, 1589-1610; b) P. Camurlu, T. Durak, A. Balan, L. Toppare, *Synth. Met.* **2011**, *161*, 1898-1905; c) S. Narayanan, S. P. Raghunathan, A. C. Poulouse, S. Mathew, K. Sreekumar, C. Sudha Kartha, R. Joseph, *New J. Chem.* **2015**, *39*, 2795-2806.
- [3] a) G. Barbarella, L. Favaretto, G. Sotgiu, M. Zambianchi, V. Fattori, M. Cocchi, F. Cacialli, G. Gigli, R. Cingolani, *Adv. Mater.* **1999**, *11*, 1375-1379; b) A. Cazzato, M. L. Capobianco, M. Zambianchi, L. Favaretto, C. Bettini, G. Barbarella, *Bioconjugate Chem.* **2007**, *18*, 318-322; c) A. B. Nepomnyashchii, R. J. Ono, D. M. Lyons, C. W. Bielawski, J. L. Sessler, A. J. Bard, *Chem. Sci.* **2012**, *3*, 2628-2638; d) M. L. Capobianco, G. Barbarella, A. Manetto, *Molecules* **2012**, *17*, 910-933.
- [4] H. Spanggaard, F. C. Krebs, *Sol. Energy Mater. Sol. Cells* **2004**, *83*, 125-146.
- [5] a) T. Verbiest, K. Clays, V. Rodriguez, *Second-order Nonlinear Optical Characterization Techniques: An Introduction*, CRC Press, New York, **2009**; b) Y. Shen, C.-F. Chen, *Chem. Rev.* **2012**, *112*, 1463-1535; c) M. Gingras, *Chem. Soc. Rev.* **2013**, *42*, 1051-1095.
- [6] D. Tilly, F. Chevallier, F. Mongin, *Synthesis* **2016**, *48*, 184-199.
- [7] F. Chevallier, M. Charlot, C. Katan, F. Mongin, M. Blanchard-Desce, *Chem. Commun.* **2009**, 692-694.
- [8] K. Clays, K. Wostyn, A. Persoons, S. Maiorana, A. Papagni, C. A. Daul, V. Weber, *Chem. Phys. Lett.* **2003**, *372*, 438-442.
- [9] T. Verbiest, A. Persoons, in *Topics in Stereochemistry*, Vol. 24 (Eds.: M. M. Green, R. J. M. Nolte, E. W. Meijer), Wiley, New York, **2003**, pp. 519-570.
- [10] a) J. Zyss, J. F. Nicoud, M. Coquillay, *J. Chem. Phys.* **1984**, *81*, 4160-4167; b) R. Andreu, I. Malfant, P. G. Lacroix, H. Gornitzka, K. Nakatani, *Chem. Mater.* **1999**, *11*, 840-848.
- [11] P. Yan, A. C. Millard, M. Wei, L. M. Loew, *J. Am. Chem. Soc.* **2006**, *128*, 11030-11031.
- [12] a) B. Champagne, J.-M. André, E. Botek, E. Licandro, S. Maiorana, A. Bossi, K. Clays, A. Persoons, *ChemPhysChem* **2004**, *5*, 1438-1442; b) A. Bossi, E. Licandro, S. Maiorana, C. Rigamonti, S. Righetto, G. R. Stephenson, M. Spassova, E. Botek, B. Champagne, *J. Phys. Chem. C* **2008**, *112*, 7900-7907; c) B. Champagne, S. N. Labidi, *Chem. Phys. Lett.* **2016**, *644*, 195-200.
- [13] E. Botek, F. Castet, B. Champagne, *Chem. Eur. J.* **2006**, *12*, 8687-8695.
- [14] M. Ohkita, J.-M. Lehn, G. Baum, D. Fenske, *Chem. Eur. J.* **1999**, *5*, 3471-3481.
- [15] a) I. Huc, *Eur. J. Org. Chem.* **2004**, 17-29; b) A. Petitjean, L. A. Cuccia, M. Schmutz, J.-M. Lehn, *J. Org. Chem.* **2008**, *73*, 2481-2495.
- [16] a) J.-M. L'Helgoual'ch, A. Seggio, F. Chevallier, M. Yonehara, E. Jeanneau, M. Uchiyama, F. Mongin, *J. Org. Chem.* **2008**, *73*, 177-183; b) K. Snégaroff, S. Komagawa, F. Chevallier, P. C. Gros, S. Golhen, T. Roisnel, M. Uchiyama, F. Mongin, *Chem. Eur. J.* **2010**, *16*, 8191-8201; c) K. Snégaroff, T. T. Nguyen, N. Marquise, Y. S. Halauko, P. J. Harford, T. Roisnel, V. E. Matulis, O. A. Ivashkevich, F. Chevallier, A. E. H. Wheatley, P. C. Gros, F. Mongin, *Chem. Eur. J.* **2011**, *17*, 13284-13297; d) M. Hedidi, G. Bentabed-Ababsa, A. Derdour, Y. S. Halauko, O. A. Ivashkevich, V. E. Matulis, F. Chevallier, T. Roisnel, V. Dorcet, F. Mongin, *Tetrahedron* **2016**, *72*, 2196-2205.
- [17] E. Marzi, A. Bigi, M. Schlosser, *Eur. J. Org. Chem.* **2001**, 1371-1376.
- [18] J. V. Mello, N. S. Finney, *Org. Lett.* **2001**, *3*, 4263-4265.
- [19] a) E.-i. Negishi, *Handbook of Organopalladium Chemistry for Organic Synthesis, Vol. 1*, Wiley-Interscience, New York, **2002**; b) A. O. King, N. Okukado, E.-i. Negishi, *J. Chem.*

- Soc., Chem. Commun.* **1977**, 683-684; c) A. Seggio, G. Priem, F. Chevallier, F. Mongin, *Synthesis* **2009**, 3617-3632.
- [20] M. Schlosser, C. Bobbio, T. Rausis, *J. Org. Chem.* **2005**, *70*, 2494-2502.
- [21] a) K. Nassau, *The Physics and Chemistry of Color: The Fifteen Causes of Color*, John Wiley & Sons, New York, **1983**; b) J. B. Birks, *Photophysics of Aromatic Molecules*, Wiley-Interscience, London, **1970**.
- [22] S. J. Strickler, R. A. Berg, *J. Chem. Phys.* **1962**, *37*, 814-822.
- [23] a) C. Xu, W. W. Webb, *J. Opt. Soc. Am. B* **1996**, *13*, 481-491; b) M. A. Albota, C. Xu, W. W. Webb, *Appl. Opt.* **1998**, *37*, 7352-7356.
- [24] a) M. Pawlicki, H. A. Collins, R. G. Denning, H. L. Anderson, *Angew. Chem., Int. Ed.* **2009**, *48*, 3244-3266; b) F. Terenziani, C. Katan, E. Badaeva, S. Tretiak, M. Blanchard-Desce, *Adv. Mater.* **2008**, *20*, 4641-4678.
- [25] K. Clays, J. Jannes, Y. Engelborghs, A. Persoons, *J. Phys. E Sci. Instrum.* **1989**, *22*, 297-305.
- [26] G. J. T. Heesink, A. G. T. Ruiter, N. F. van Hulst, B. Bölger, *Phys. Rev. Lett.* **1993**, *71*, 999-1002.
- [27] J. L. Oudar, D. S. Chemla, *J. Chem. Phys.* **1977**, *66*, 2664-2668.
- [28] K. Clays, K. Wostyn, G. Olbrechts, A. Persoons, A. Watanabe, K. Nogi, X.-M. Duan, S. Okada, H. Oikawa, H. Nakanishi, H. Vogel, D. Beljonne, J.-L. Brédas, *J. Opt. Soc. Am. B* **2000**, *17*, 256-265.
- [29] L. Severa, D. Koval, P. Novotná, M. Ončák, P. Sázelová, D. Šaman, P. Slavíček, M. Urbanová, V. Kašička, F. Teplý, *New J. Chem.* **2010**, *34*, 1063-1067.
- [30] H. E. Gottlieb, V. Kotlyar, A. Nudelman, *J. Org. Chem.* **1997**, *62*, 7512-7515.
- [31] a) G. A. Crosby, J. N. Demas, *J. Phys. Chem.* **1971**, *75*, 991-1024; b) D. F. Eaton, *Pure Appl. Chem.* **1988**, *60*, 1107-1114.
- [32] K. Clays, A. Persoons, *Phys. Rev. Lett.* **1991**, *66*, 2980-2983.
- [33] G. Olbrechts, R. Strobbe, K. Clays, A. Persoons, *Rev. Sci. Instrum.* **1998**, *69*, 2233-2241.
- [34] K. Wostyn, K. Binnemans, K. Clays, A. Persoons, *Rev. Sci. Instrum.* **2001**, *72*, 3215-3220.
- [35] S. Grimme, *J. Comput. Chem.* **2006**, *27*, 1787-1799.
- [36] a) H. Iikura, T. Tsuneda, T. Yanai, K. Hirao, *J. Chem. Phys.* **2001**, *115*, 3540-3544; b) Y. Tawada, T. Tsuneda, S. Yanagisawa, T. Yanai, K. Hirao, *J. Chem. Phys.* **2004**, *120*, 8425-8433.
- [37] H. Stoll, A. Savin, in *Density Functional Methods in Physics* (Eds.: R. M. Dreizler, J. da Providencia), Plenum, New York, **1985**, pp. 177-208.
- [38] a) M. Kamiya, H. Sekino, T. Tsuneda, K. Hirao, *J. Chem. Phys.* **2005**, *122*, 23411101-23411110; b) H. Sekino, Y. Maeda, M. Kamiya, K. Hirao, *J. Chem. Phys.* **2007**, *126*, 0141071-0141076; c) P. A. Limacher, K. V. Mikkelsen, H. P. Lüthi, *J. Chem. Phys.* **2009**, *130*, 1941141-1941147; d) M. de Wergifosse, B. Champagne, *J. Chem. Phys.* **2011**, *134*, 07411301-07411313; e) S.-I. Lu, C.-C. Chiu, Y.-F. Wang, *J. Chem. Phys.* **2011**, *135*, 1341041-1341047.
- [39] L. Kronik, T. Stein, S. Refaely-Abramson, R. Baer, *J. Chem. Theory Comput.* **2012**, *8*, 1515-1531.
- [40] a) H. Sun, J. Autschbach, *ChemPhysChem* **2013**, *14*, 2450-2461; b) K. Garrett, X. A. Sosa Vazquez, S. B. Egri, J. Wilmer, L. E. Johnson, B. H. Robinson, C. M. Isborn, *J. Chem. Theory Comput.* **2014**, *10*, 3821-3831; c) M. Hidalgo Cardenuto, B. Champagne, *Phys. Chem. Chem. Phys.* **2015**, *17*, 23634-23642.
- [41] a) J. Tomasi, M. Persico, *Chem. Rev.* **1994**, *94*, 2027-2094; b) J. Tomasi, B. Mennucci, R. Cammi, *Chem. Rev.* **2005**, *105*, 2999-3093.
- [42] R. Bersohn, Y.-H. Pao, H. L. Frisch, *J. Chem. Phys.* **1966**, *45*, 3184-3198.
- [43] M. J. Frisch, G. W. Trucks, H. B. Schlegel, G. E. Scuseria, M. A. Robb, J. R. Cheeseman, G. Scalmani, V. Barone, B. Mennucci, G. A. Petersson, H. Nakatsuji, M. Caricato, X. Li, H. P. Hratchian, A. F. Izmaylov, J. Bloino, G. Zheng, J. L. Sonnenberg, M. Hada, M. Ehara, K.

Toyota, R. Fukuda, J. Hasegawa, M. Ishida, T. Nakajima, Y. Honda, O. Kitao, H. Nakai, T. Vreven, J. A. Montgomery, Jr., J. E. Peralta, F. Ogliaro, M. Bearpark, J. J. Heyd, E. Brothers, K. N. Kudin, V. N. Staroverov, R. Kobayashi, J. Normand, K. Raghavachari, A. Rendell, J. C. Burant, S. S. Iyengar, J. Tomasi, M. Cossi, N. Rega, J. M. Millam, M. Klene, J. E. Knox, J. B. Cross, V. Bakken, C. Adamo, J. Jaramillo, R. Gomperts, R. E. Stratmann, O. Yazyev, A. J. Austin, R. Cammi, C. Pomelli, J. W. Ochterski, R. L. Martin, K. Morokuma, V. G. Zakrzewski, G. A. Voth, P. Salvador, J. J. Dannenberg, S. Dapprich, A. D. Daniels, Ö. Farkas, J. B. Foresman, J. V. Ortiz, J. Cioslowski, D. J. Fox, *Gaussian 09*, Revision A.1, Gaussian, Inc., Wallingford CT, **2009**.

Table 1. Photophysical and two-photon absorption data of oligomers **1-4** in chloroform and their analogues lacking an heptynyl chain (**1'-3'**).^[7]

| | $\lambda_{\text{abs}}^{\text{max3}}$ (nm) | $10^{-4} \epsilon^{\text{max3}}$ ($\text{cm}^{-1} \text{M}^{-1}$) | $\lambda_{\text{abs}}^{\text{max2}}$ (nm) | $10^{-4} \epsilon^{\text{max2}}$ ($\text{cm}^{-1} \text{M}^{-1}$) | $\lambda_{\text{abs}}^{\text{max1}}$ (nm) | $10^{-4} \epsilon^{\text{max1} b}$ ($\text{cm}^{-1} \text{M}^{-1}$) | $\lambda_{\text{em}}^{\text{max}}$ (nm) | Φ_f^a (%) | Φ_{Δ}^b (%) | τ_f^c (ns) | $10^{-9} k_r^d$ (s^{-1}) | $10^{-9} k_{\text{nr}}^d$ (s^{-1}) | $2\lambda_{\text{max1}}$ | $\lambda_{\text{TPA}}^{\text{max3}}$ (nm) | σ_2^{max3} (GM) | $\lambda_{\text{TPA}}^{\text{max2}}$ (nm) | σ_2^{max2} (GM) | $\lambda_{\text{TPA}}^{\text{max1}}$ (nm) | σ_2^{max1} (GM) |
|-----------|--|--|--|--|--|--|--|-------------------|--------------------------|--------------------|--|--|--------------------------|--|----------------------------------|--|----------------------------------|--|----------------------------------|
| 1 | 257 | 2.03 | 286 | 1.55 | 334 | 1.38 | 391 | 3.1 | | 0.36 | 0.09 | 2.69 | 668 | - | | - | | - | |
| 1' | | | 286 | 1.22 | 315.5 | 1.71 | 372 | 1.3 | 47 | 0.36 | 0.04 | 2.74 | | | | | | | |
| 2 | 309 | 2.55 | 354 | 2.59 | 388(sh),402 | 3.03 | 437 | 34 | 35 | 1.2 | 0.28 | 0.54 | 804 | <700 | 40 | 720 | 40 | 810 | 8 |
| 2' | 299 | 2.49 | 343 | 2.30 | 373,389(sh) | 3.12 | 408 | 15 | 85 | 0.5 | 0.29 | 1.67 | | | | | | | |
| 3 | 322 | 3.98 | 365 | 4.62 | 402, 415(sh) | 3.23 | 439,464(sh) | 40 | 28 | 2.2 | 0.18 | 0.27 | 804 | <700 | 70 | 750 | 50 | 810 | 13 |
| 3' | 310 | 3.47 | 353 | 3.62 | 390 | 3.11 | 426,450(sh) | 41 | 56 | 1.95 | 0.21 | 0.30 | | | | | | | |
| 4 | 329 | 5.76 | 391 | 5.31 | 420 sh | 3.57 | 444,472(sh) | 29 | 25 | 2.45 | 0.12 | 0.29 | 840 | <700 | 105 | 750 | 50 | 820 | 15 |

^a Fluorescence quantum yield determined in chloroform relative to quinine in 0.5 M H₂SO₄. ^b Singlet oxygen quantum yield determined relative to tetraphenylporphyrin. ^c Experimental fluorescence lifetime. ^d Radiative (k_r) and non-radiative (k_{nr}) decay rates. ^e Two-photon absorption maxima. ^f Two-photon absorption cross-section (1GM= $10^{50} \text{ cm}^4 \cdot \text{s} \cdot \text{photon}^{-1}$)

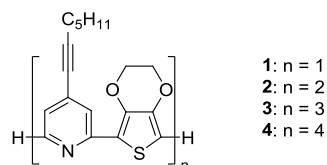
Table 2. Second-order nonlinear optical properties of chromophores **1-4**: dynamic fluorescence-free first hyperpolarizability, $\beta_{\text{HRS},880}$; estimated static fluorescence-free first hyperpolarizability, $\beta_{\text{HRS},0}$; parameters used in this estimation: resonance wavelength, λ_{max} ; derived resonance enhancement factor, EF; parameters from TPEF contribution: amplitude, A_{TPEF} ; and lifetime, τ ; and depolarization ratios ρ : *at low frequency (1 kHz, TPEF affected), at indicated high frequency (^a: 320 MHz, ^b: 880 MHz, still TPEF affected), and as derived from global fitting.* As a reference for the ρ values, the octopolar crystal violet chloride is used, resulting in ρ values of 1.47 at 1 kHz, 1.43 at 320 MHz and 1.55 at 880 MHz, or essentially 1.5 as expected for the octopole.

| | $\beta_{\text{HRS},880}$ (10^{-30} esu) | λ_{max} (nm) | EF | $\beta_{\text{HRS},0}$ (10^{-30} esu) | τ (ns) | A_{TPEF} (10^{-30} esu) | ρ 1 kHz | $\rho^{\text{a,b}}$ MHz | ρ global fit |
|----------|---|--------------------------------|-------|---|----------------|--|-----------------|----------------------------|----------------------|
| 1 | 63 ± 5 | 333 | 2.73 | 23 ± 2 | 1.0 ± 0.2 | 70 ± 4 | 1.06 ± 0.2 | $1.12 \pm 0.2^{\text{a}}$ | NA |
| 2 | 350 ± 180 | 402 | 7.65 | 46 ± 23 | 2.0 ± 0.3 | 2680 ± 80 | 1.09 ± 0.2 | $1.71 \pm 0.2^{\text{b}}$ | 4 ± 2 |
| 3 | 1130 ± 130 | 415 | 11.65 | 96 ± 11 | 3.0 ± 0.3 | 6000 ± 200 | 1.05 ± 0.2 | $1.78 \pm 0.2^{\text{b}}$ | 3 ± 2 |
| 4 | 1550 ± 150 | 420 | 14.58 | 106 ± 10 | 3.0 ± 0.2 | 8000 ± 200 | 1.06 ± 0.2 | $1.49 \pm 0.2^{\text{b}}$ | 2 ± 1 |

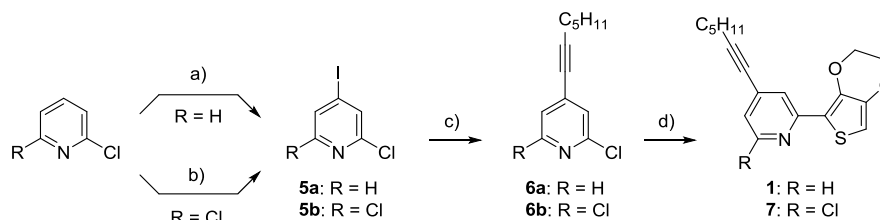
NA: not available, not enough signal and not even an onset of increase in ρ value for higher AM frequencies, since shortest fluorescence lifetime τ , as also to be observed in Figure SI1 lower panel.

Table 3. EFISHG first hyperpolarizability values, $\beta_{//}$; HRS first hyperpolarizability values, β_{HRS} ; and depolarization ratios, ρ ; for increasingly large DA_n ($n = 1-5$) helices calculated at the IEF-PCM/TDDFT/LC-BLYP level of approximation with the 6-311+G(d) basis sets and at $\lambda = 1064$ nm.

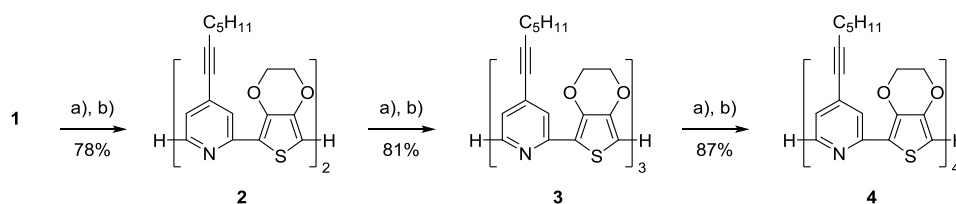
| n | $\beta_{//}$ (10^{-30} esu) | β_{HRS} (10^{-30} esu) | ρ |
|---|--------------------------------|--|--------|
| 1 | 2.9 | 4.1 | 4.68 |
| 2 | 5.0 | 6.2 | 2.20 |
| 3 | 3.6 | 8.2 | 1.73 |
| 4 | 3.1 | 10.7 | 1.58 |
| 5 | 3.4 | 10.9 | 1.61 |



Scheme 1.



Scheme 2. a) $\text{ZnCl}_2 \cdot \text{TMEDA}$ (0.5 equiv), $[\text{Li}(\text{tmp})]$ (1.5 equiv), THF, RT, 2 h, then I_2 , then ${}^i\text{Pr}_2\text{NLi}$, THF, -75°C , 4 h (**5a**, 51%). b) ${}^n\text{BuLi}$, THF, -75°C , 45 min, then I_2 (**5b**, 56%). c) 1-heptyne, Et_2NH , CuI (10 mol%), $\text{PdCl}_2(\text{PPh}_3)_2$ (5 mol%), THF, RT, 12 h (**6a**, 98%; **6b**, 99%). d) EDOT, ${}^n\text{BuLi}$, $\text{ZnCl}_2 \cdot \text{TMEDA}$, PdCl_2 (2 mol%), dppf (2 mol%), THF, reflux, 48 h (**1**, 88%; **7**, 73%).



Scheme 3. a) ${}^n\text{BuLi}$, then $\text{ZnCl}_2 \cdot \text{TMEDA}$, THF, 0°C , 1 h. b) **7**, PdCl_2 (2 mol%), dppf (2 mol%), reflux, 48 h.

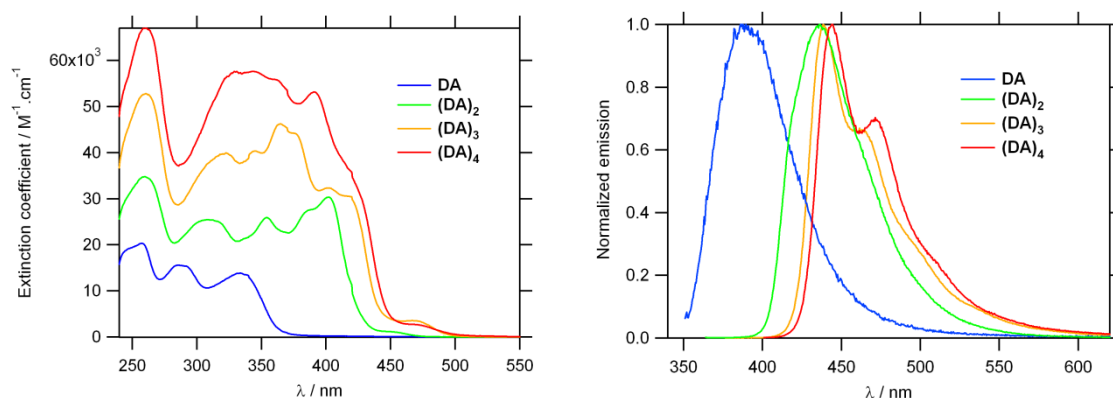


Figure 1. Absorption spectra (left panel) and normalized emission spectra (right panel) of 4 EDOT-ethynylpyridine oligomers **1-4** in CHCl_3 .

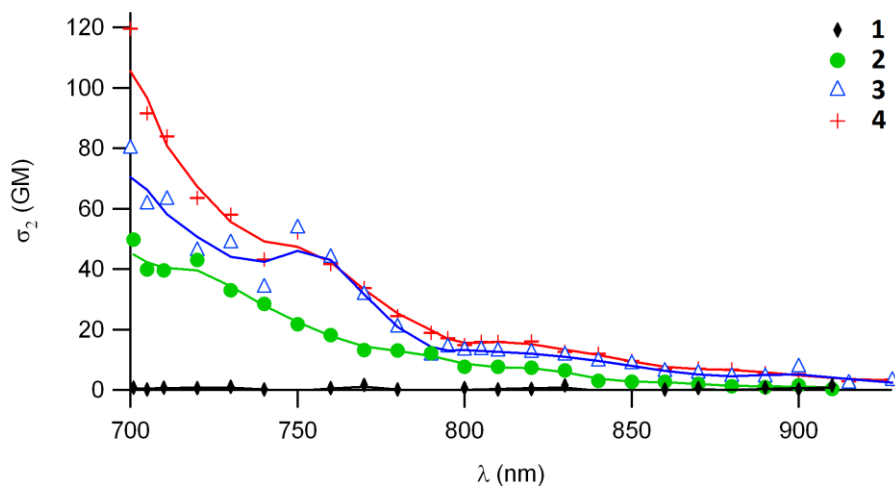


Figure 2. Two-photon absorption spectra of EDOT-ethynylpyridine oligomers **1-4** in CHCl_3 .

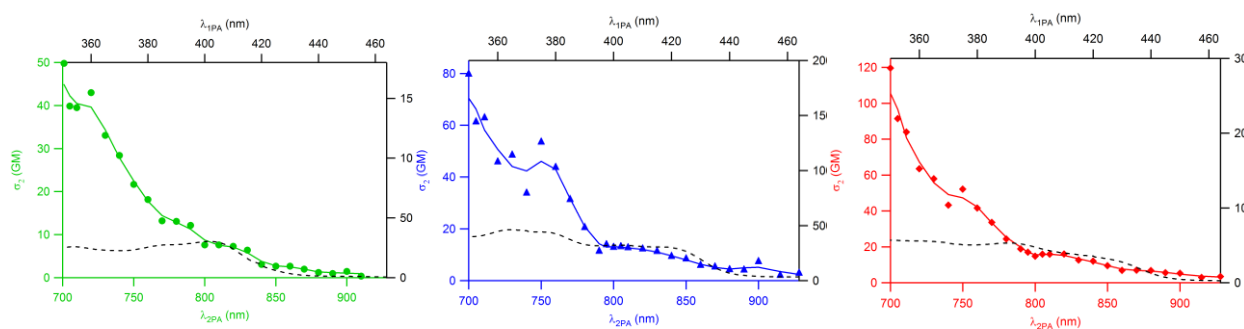


Figure 3. Two-photon absorption spectra of compound **2** (left), **3** (middle) and **4** (right) compared with their rescaled one-photon absorption spectra.

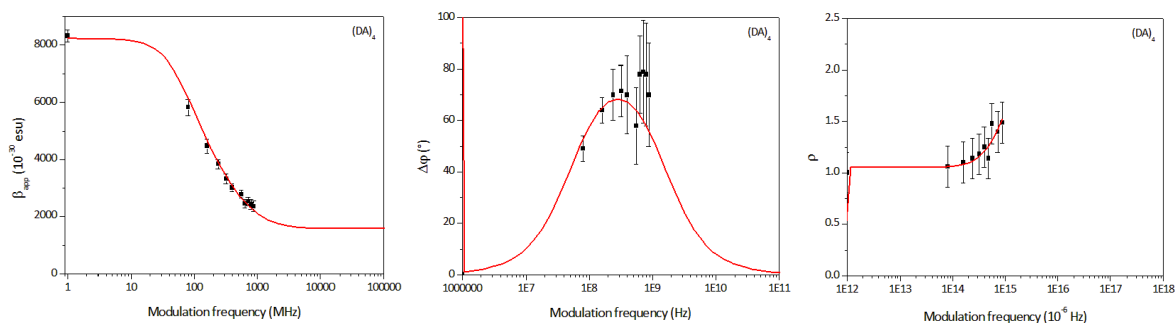


Figure 4. Experimental results from hyper-Rayleigh scattering for compound **4** in CHCl_3 at 880 nm: Data (black) points: left panel: demodulation of the AM frequency-dependent apparent first hyperpolarizability; middle panel: phase lag between pure scattering from non-fluorescent reference and total signal; right panel: AM frequency dependence of HRS depolarization ratio. Solid (red) line: fitting towards single fluorescence lifetime, τ , TPEF amplitude, A_{TPEF} , and fluorescence-free first hyperpolarizability β_{HRS} . Results for compounds **1** to **3** are provided in the Supporting Information section.

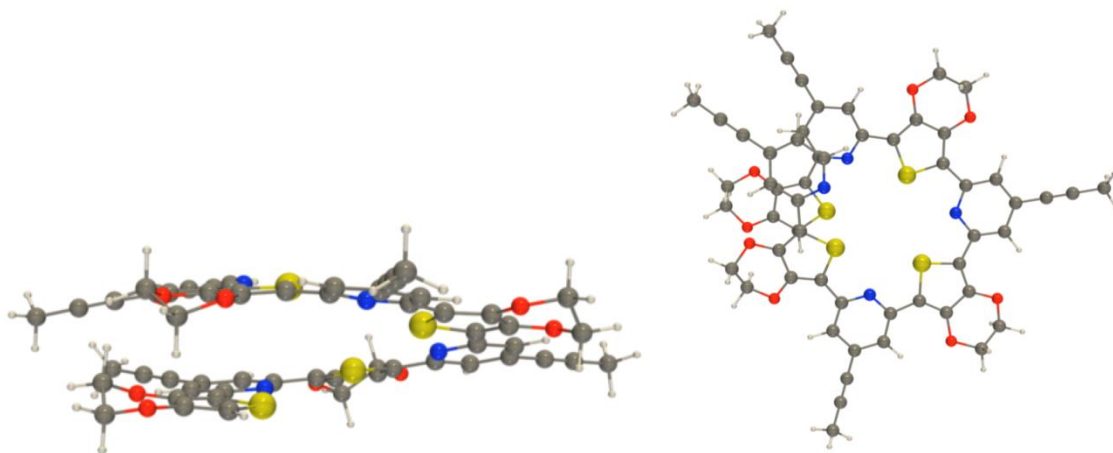


Figure 5. Lateral and top views of the B97-D/6-311G(d) optimized structure of compound **4**.

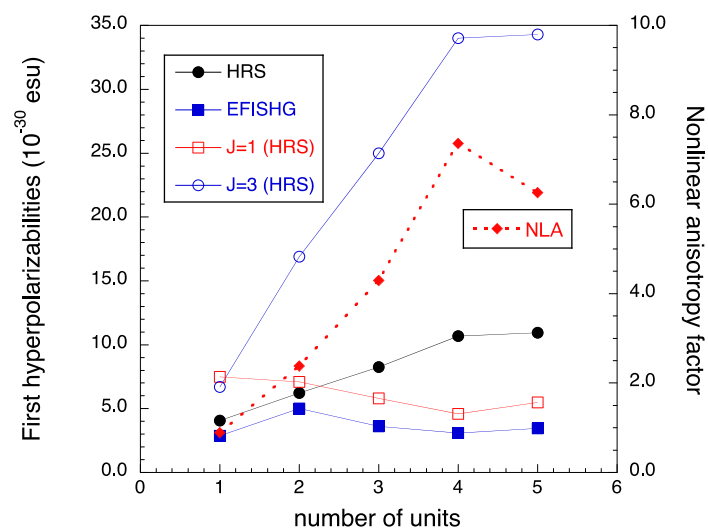
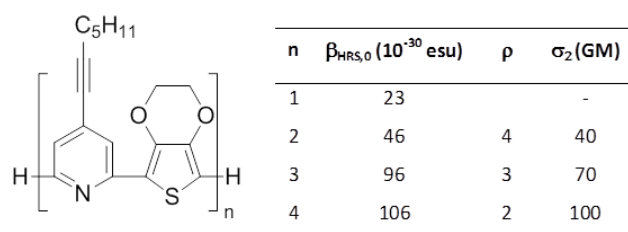


Figure 6. HRS (β_{HRS} , $\beta_{\text{J=1}}$, $\beta_{\text{J=3}}$, and NLA) and EFISHG (β_{\parallel}) quantities as a function of the number of units calculated at the IEF-PCM/TDDFT/LC-BLYP/6-311+G(d) level of approximation at $\lambda = 1064$ nm.

TOC



dipolar planar \longrightarrow octupolar/helicoidal

Alternated 3,4-ethylenedioxythiophene-alkynylpyridine oligomers $(\text{DA})_n$ were shown to undergo transition from linear dipolar structures ($n=1-2$) to coiled octupolar structures ($n>2$) as demonstrated by hyper-Rayleigh scattering experiments and calculations. The transition from linear to coiled structure also leads to sizeable two-photon absorption response at 700 nm.